IOPscience iopscience.iop.org

Home Search Collections Journals About Contact us My IOPscience

A Fourier transform spectrometer using resonant vertical comb actuators

This content has been downloaded from IOPscience. Please scroll down to see the full text.

2006 J. Micromech. Microeng. 16 2517

(http://iopscience.iop.org/0960-1317/16/12/001)

View the table of contents for this issue, or go to the journal homepage for more

Download details:

IP Address: 212.175.32.131
This content was downloaded on 26/08/2014 at 08:26

Please note that terms and conditions apply.

J. Micromech. Microeng. **16** (2006) 2517–2523 doi:10.1088/0960-1317/16/12/001

A Fourier transform spectrometer using resonant vertical comb actuators

Caglar Ataman, Hakan Urey and Alexander Wolter

Koc University, Optical Microsystems Laboratory, Rumeli Feneri Yolu, 34450 Sariyer, Istanbul, Turkey
and
Fraunhofer Institute for Photonic Microsystems, Maria-Reiche-Str. 201109 Dresden, Germany

E-mail: cataman@ku.edu.tr, hurey@ku.edu.tr and alexander.wolter@ipms.fraunhofer.de

Received 25 May 2006, in final form 7 September 2006
Published 10 October 2006
Online at stacks.iop.org/JMM/16/2517

Abstract
The design, fabrication and characterization of a novel out-of-plane vertical comb-drive actuator based lamellar grating interferometer (LGI) is reported. The interferometer utilizes resonant mode vertical comb actuators, where comb fingers are simultaneously used for actuation and as a movable diffraction grating, making the device very compact. The Fourier transform of the zeroth order intensity pattern as a function of the optical path difference gives the spectrum of light. The main advantages offered by the proposed device are a long travel range (i.e. good spectral resolution), a large clear aperture (i.e. high light efficiency), and a very simple, robust and compact spectrometer structure. Peak-to-peak 106 μm out-of-plane deflection is observed in ambient pressure and at 28 V, corresponding to a theoretical spectral resolution of about 0.4 nm in the visible band and 3.6 nm at 1.5 μm. A simple CMOS compatible process based on bulk micromachining of a silicon-on-insulator wafer is used for the device fabrication.

1. Introduction

A Fourier transform spectrometer (FTS) is a Michelson interferometer with a movable reference mirror. The invention of this method dates back to 1880 and coincides with the invention of the Michelson interferometer [1]. However, due to the lack of available technology, FTS did not become a common interferometric measurement technique, until recently. Fast detector arrays, efficient Fourier transform algorithms and the increasing computing power of microprocessors enabled FTS to become a well-known and widely used measurement technique, particularly for the infrared band. A lamellar grating interferometer (LGI) is a special type of FTS that utilizes a movable diffraction grating and operates in the zeroth order [2]. The interfering wavelets are formed by the division of the wavefront by the grating; while in Michelson configuration, the wave amplitude is split with a beam splitter. Simpler operation principle and fewer optical components of LGI make it possible to build very compact and robust spectrometers with good performance.

The movable diffraction grating used for the LGI should provide a sufficiently large travel range for high resolution and a small grating period for elimination of the cross-talk between diffraction orders. MOEMS technology offers very precise and high volume fabrication capabilities for micron scale movable gratings. Therefore a significant amount of research is done to develop compact and relatively high-resolution microspectrometer devices based on the MOEMS technology. Kenda [3] demonstrated a FTS in mid-IR using Michelson interferometer configuration where an additional reference mirror, IR beamsplitter, and vacuum packaging are needed. Schenk [4] demonstrated a scanning spectrometer on a silicon-on-insulator (SOI) wafer with special crystal orientation where a blazed grating is etched on the top surface of a torsional MEMS scanner. The system has good efficiency and performance but requires special wafers and a compromise between the detector size and the spectral resolution. Manzardo [5, 6] demonstrated an LGI-based FTS. The structure uses side walls of thick SOI wafers; however, surface roughness and side-wall thickness limitations imposes tight opto-mechanical tolerances and light collection efficiency

0960-1317/06/122517+07$30.00 © 2006 IOP Publishing Ltd Printed in the UK

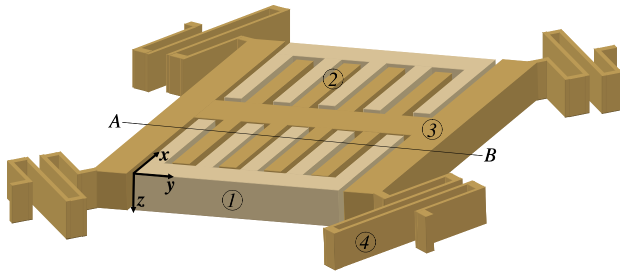

Figure 1. Spectrometer device structure. (1) Fixed fingers, (2) movable fingers, (3) rigid backbone, (4) folded flexures. (The figure is not drawn according to actual proportions.)

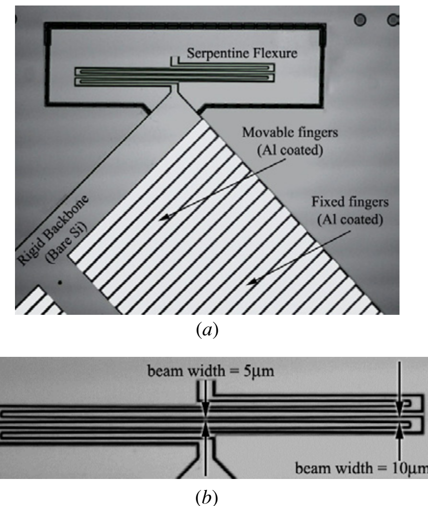

Figure 2. (*a*) Microscope image of the fabricated device. The high-reflectivity light color areas are the aluminum coated reflective comb fingers; other areas are bare silicon. (*b*) Close-up view of the serpentine flexure; the non-uniform beam cross section has a width of 5 μm and 10 μm at the center and the ends of the beam, respectively.

limitations and requires the use of anamorphic optics for illuminating the thin and long mirror area.

In this work, a novel FTS system based on out-of-plane vertical resonant comb actuators using simple fabrication on standard SOI wafers is presented. The comb fingers have dual functionality and are used both for actuation and dynamic diffraction grating, which greatly reduces the die size and eliminates the use of a beam splitter and other IR optics. Since only a single reflector surface is used between the source and the detector, the system operation is broadband and suitable for visible, mid-wave and long-wave infrared bands at the same time. In addition, the light collection surface of the design is the top surface of the wafer; therefore good surface quality and high light efficiency can be achieved. Due to the out-of plane actuation, the travel range of the fingers is not limited by the length of the comb fingers and the device operates without vacuum packaging.

Structural properties and operation principle of the movable grating are presented in section 2 and 3, respectively. An optical performance analysis of the spectrometer is discussed in section 4. In section 5, we present the experimental characterization results of the device.

2. Device structure

2.1. Mechanical design

An illustration of the grating structure designed for this application and a photograph of the actual device are shown in figures 1 and 2(*a*), respectively. At the core of the structure, there are two sets of electrostatic comb fingers that are simultaneously utilized as an actuator and a variable-depth diffraction grating. The comb sets are symmetrically placed on a rigid backbone, which enhances the robustness of the structure and helps to keep the device surface flat while resonating. The width and length of these comb fingers (both static and movable) are 70 μm and 1.2 mm, respectively, where the gap between them is 5 μm. A high width-to-gap ratio of the comb fingers ensures a high fill factor and therefore, good optical efficiency; however, it also increases the grating period, which is unfavorable due to smaller separation between diffraction orders. The comb fingers are coated with a 100 nm thick layer of aluminum, hence, the reflectivity of the fingers is enhanced for the visible and infrared region, allowing broadband operation. The 250 μm wide H-shaped backbone that carries the movable fingers is connected to the fixed frame via four folded flexure beams. Figure 2(*b*) is a close-up view of one of the folded flexures which have varying cross-sectional width to have uniform stress distribution and to provide low stiffness within a compact structure [7]. Low stiffness springs lower the resonant frequency and speed requirements of the readout electronics, and increase the travel range, which improves the spectral resolution.

2.2. Fabrication

The spectrometer is fabricated on a silicon-on-insulator wafer with a CMOS compatible process. The 30 μm thick structural layer is highly doped to maintain conductivity. The fundamental steps of the fabrication process are shown in figure 3. For the definition of wire-bond electrodes, an oxide and a metal layer is deposited on the structural layer and then patterned (not shown in the figure). On the backside of the wafer a hard mask consisting of an oxide and a silicon nitride layer is deposited and patterned for a further backside etching step (figure 3(*a*)). Then, a 100 nm thick aluminum layer is deposited on the movable and fixed fingers to enhance reflectivity (figure 3(*b*)). The substrate under the mechanical elements and the buried oxide are subsequently etched away in a TMAH and an HF solution (figure 3(*c*)). Finally, the mechanical elements are released by an ASE™ deep silicon etching process (figure 3(*d*)).

2.3. Actuation principle

Electrostatic comb drive actuation is frequently used in MEMS systems, since very high force densities can be obtained with this method. Rotational micromirros [8, 9], and in-plane/out-of-plane translational micro-stages [10] are some of the common devices that employ comb actuation in various degree-of-freedoms (DOFs). In resonance, the operation mode of the comb-actuated device is determined by the excitation frequency and the eigenmodes of the mechanical structure. By

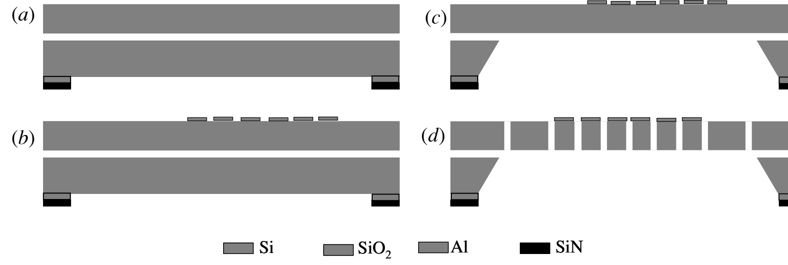

Figure 3. Schematic process flow. The drawings correspond to a cross-section along the line A–B defined in figure 1.

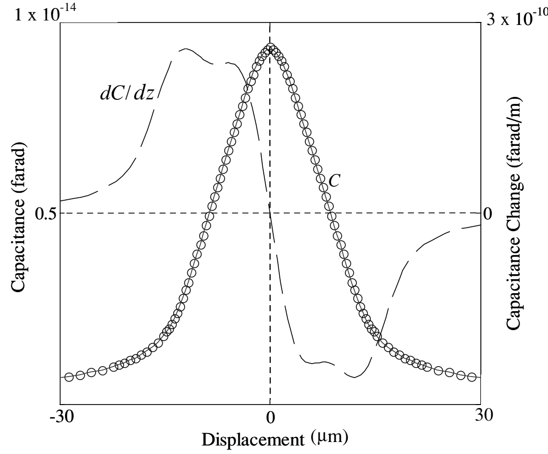

Figure 4. Capacitance versus deflection curve and its derivative for a single comb finger. A high-order polynomial is fitted to the FEA simulation data of the capacitance curve.

Table 1. Experimental and FEA mode frequency results. Experimental data for the fourth and fifth modes are not available due to the lack of in-plane measurement equipment.

Mode frequencies (Hz)	*FEA* (Hz)	Exp. (Hz)
Out-of-plane translation (along -*z*)	1156	1111
Rotation (around *x*)	1913	1885
Rotation (around *y*)	2230	2140
In-plane translation (along *x*)	3890	–
In-plane translation (along *y*)	4510	–

varying the excitation frequency, a comb-actuated structure can be oscillated in different mechanical eigenmodes.

Table 1 lists the experimental and simulated eigenmode frequencies for the movable grating structure. The out-of-plane translation mode, functional for the spectrometer application, is located at around 1.1 kHz, and is sufficiently away from the second eigenmode enabling mono-mode oscillation. Hence, a single DOF model for the device can be established using the following standard equation of motion [11]:

$$I_m \frac{d^2 z}{dt^2} + b\frac{dz}{dt} + K_f z = F(z,t), \quad (1)$$

where, I_m is the inertial mass, b is the damping constant, K_f is the mechanical stiffness, and F is the time and position dependent force, which can be expressed as

$$F(z,t) = N\frac{dC}{dz}V(t)^2, \quad (2)$$

where N is the total number of comb fingers on both sides of the device, C is the capacitance of a single finger, and $V(t)$ is the drive voltage. Figure 4 shows the capacitance displacement and rate of change of capacitance with respect to displacement for a single finger of a vertical comb actuator obtained using FEMLAB™. Despite the displacement independent force of in-plane mode comb drives, the torque induced by the out-of-plane mode comb actuators is strongly dependent on the displacement. As is discussed in detail in [12], if the force expression in (2) is expanded as a Taylor series and the excitation signal is chosen to be a squared-root sinusoid ($V(t) = A\sqrt{\cos(wt)+1}$) for mathematical convenience, the force induced by the comb actuator can be expressed as

$$F(z,t) = -(r_1 z + r)3z^3 + r_5 z^5 + \cdots)A^2(\cos(wt)+1), \quad (3)$$

where r_i are the Taylor series coefficients of the deflection derivative of the capacitance function, which has only odd terms. Thus, the equation of motion becomes

$$I_m \frac{d^2 z}{dt^2} + b\frac{dz}{dt} + (K_f + r_1 A^2(\cos(\omega t)+1))z + (r_3 A^2(\cos(\omega t)+1))z^3 + \cdots = 0. \quad (4)$$

The right-hand side of (4) has no constant force term; hence the system does not respond to dc excitation. This can also be observed from the symmetry of the structure in figure 1. The time-dependent excitation of the equation of motion appears as the coefficients (parameters) of the equation of motion, which leads to time modulation of the stiffness and nonlinearity terms. Such systems are called *parametrically excited systems* and exhibit more complicated dynamic behavior compared to linear second-order systems. A small parametric excitation can produce a large response when frequency of the excitation is close to twice the natural frequency (f_r) of the system (principal parametric resonance) or an integer fraction of $2f_r$. The resonance around $2f_r/n$ is called the nth-order parametric resonance. Hence, the excitation signal frequency should be around twice the mechanical eigenmode frequency (2.2 kHz in this case) in order to obtain maximum deflection from the device. The dynamic behavior of parametrically excited MEMS systems is examined in detail elsewhere [12–14].

3. Spectrometer operation principle

One of the major advantages of the LGI is its simple and robust operation principle. A fully functional spectrometer system can be constructed using the presented MEMS device, a single photodetector and electronic circuitry for processing the detector output, as illustrated in figure 5.

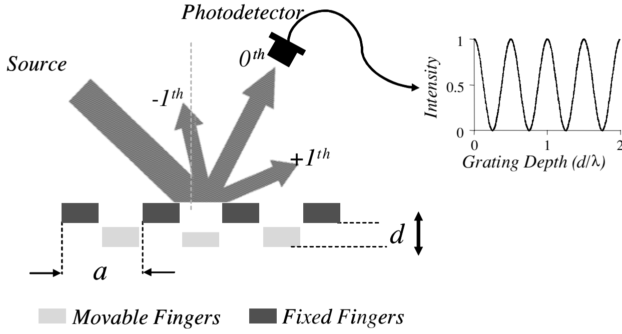

Figure 5. Schematic of a comb-drive rectangular diffraction grating, and modulation of the zeroth order intensity as d changes; the photodiode intensity is sinusoidally modulated when the illumination is assumed to be monochromatic.

When perpendicularly illuminated with monochromatic light of wavelength λ, the far-field intensity profile of the light diffracted from the grating is given by the following expression [5]:

$$I(\theta) = B \underbrace{\left(\frac{\sin(\alpha/2)}{\alpha/2}\right)^2}_{I_1} \underbrace{\left(\frac{\sin(N\alpha)}{\sin(\alpha)}\right)}_{I_2} \underbrace{\cos^2\left(\frac{4\pi d}{\lambda}\right)}_{I_3},$$
$$\alpha = \frac{\pi a}{2\lambda}\sin(\theta), \tag{5}$$

where θ is the diffraction angle, N is the number of illuminated periods, and B is a scaling factor depending on the structure dimensions. The total intensity has three distinct components. The first term (I_1) has 'sinc' shaped profile, due to the rectangular shape of the grating. The width of I_1 is inversely proportional to the period of the gratings, since it is simply the square of the Fourier transform of the grating shape. I_2 is a sinc train, resulting from the periodicity of the grating. The grating period determines the angular separation between the peaks and number of illuminated grating fingers determines the width of each peak. I_3 is the only term that modulates the intensity based on the amount of phase difference introduced by the grating.

Figure 6 is a plot of (5) for three different optical path difference (OPD) between the light reflected from the movable and fixed fingers assuming monochromatic illumination. Note that OPD is twice the grating depth due to reflection. For OPD = 0, the grating acts as a mirror and all reflected light is directed to the zeroth order. When OPD is equal to quarter of a wavelength, zeroth order intensity becomes zero, and all light goes to the higher orders.

At the center of the diffraction plane, two of the three intensity components of (5)—I_1 and I_2—are equal to 1. This can be mathematically seen by setting the diffraction angle θ to zero in (5). The resultant intensity function can be written as

$$I_{\text{center}} = B\cos^2\left(\frac{4\pi d}{\lambda}\right) = \frac{B}{2}\left(\cos\left(\frac{8\pi d}{\lambda}\right) + 1\right). \tag{6}$$

Equation (6) implies that at the center of the diffraction plane, modulation of the light intensity is sinusoidal with respect to the OPD introduced by the grating. Therefore, while the movable fingers of the spectrometer are resonating, the intensity recorded by a single photodetector placed at

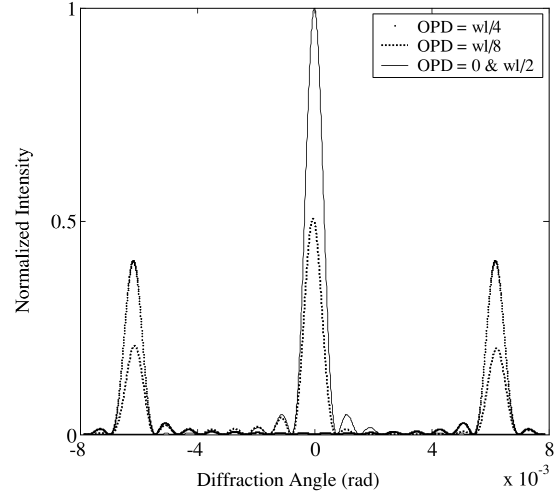

Figure 6. Intensity profile of the diffracted monochromatic light at $\lambda = ?$ in the far-field with OPD in units of wl ($= \lambda$) as the parameter. The grating period is 145 μm, which yields a diffraction angle about 6.5 mrad. If the number of illuminated periods is sufficient, isolated monitoring of the zeroth order is easily achievable.

the center of the diffraction profile with respect to grating depth would be a raised cosine with a period of $\lambda/4$. A Fourier transform operation performed on this signal would directly lead to the wavelength of the illuminating light. The dc component of the Fourier transform does not carry any information about the source; hence the measured spectrum is solely dependent on the non-dc components. The same principle can also be used for the spectral analysis of broadband sources.

4. Optical performance analysis

Spectral resolution and light efficiency are the two most important performance metrics for a spectrometer. The use of the polished top surface and out-of-plane actuation produces a large clear aperture (3 mm × 3 mm) for the incident beam. Since the structure utilizes the zeroth order diffracted light without requiring additional optics or beam splitters, the theoretical optical efficiency is >80%. As the detector can typically be oversized without compromising the spectral resolution, the efficiency is limited only by the fill-factor of the comb fingers. Therefore, the efficiency of the presented device is expected to be better than its counterparts.

The spectral resolution of the spectrometer is wavelength dependent and is fundamentally limited by the Fourier transform operation, which has to be performed on a signal of finite span. A typical intensity versus OPD signal for monochromatic light is given in figure 7. This signal is the multiplication of an infinite span raised cosine and a finite window function, and it can be mathematically represented as follows:

$$I_t(z) = \frac{B}{2}\left(\cos\left(\frac{8\pi z}{\lambda}\right) + 1\right)\text{rect}\left(\frac{z}{d_{\max}}\right), \tag{7}$$

where rect represent a rectangle function and $d_{\max}$ is the peak-to-peak travel range of the fingers. The Fourier transform of

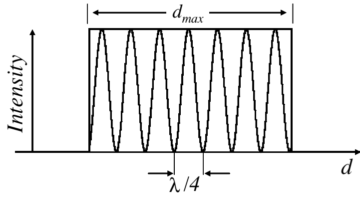

Figure 7. Typical intensity versus displacement for one period of the movable fingers.

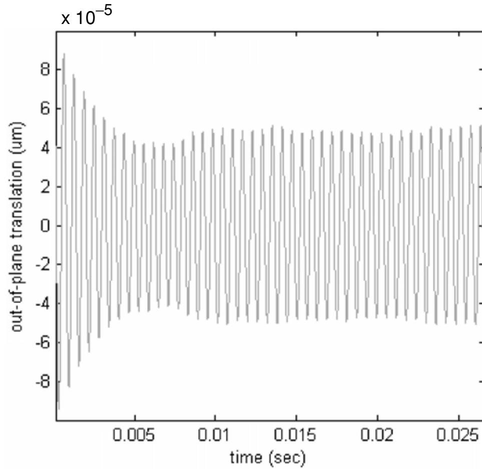

Figure 8. Transient response of the spectrometer. At 28 V, steady state travel range is ±53 μm. Due to the displacement dependant force of the comb actuators, the resulting system is a parametric oscillator.

(7) is given by

$$\Im(I_t(z)) = \frac{B}{4}\left(\delta\left(u - \frac{4}{\lambda}\right) + \delta\left(u + \frac{4}{\lambda}\right) + 2\delta(u)\right) * \frac{\sin(ud_{\max})}{\pi u d_{\max}}, \tag{8}$$

where, $*$ denotes the convolution operation. Equation (8) represents three *sinc* functions located at dc and $\pm 4/\lambda$. The resolution of the spectrometer is limited by the width of these sinc functions and can be computed by the following formula:

$$\frac{\Delta f}{f} = \frac{\Delta\lambda}{\lambda} = 0.17\frac{\lambda}{d_{\max}}, \tag{9}$$

where, f and λ are the frequency and the wavelength of the measured light and Δf and $\Delta\lambda$ are the minimum resolvable band-width and line-width of the spectrometer, respectively. Note that the resolvable width of the sinc function is based on its full-width at half-maximum (FWHM). Equation (9) implies that the resolution improves linearly with increasing travel range. This is the main motivation behind maximizing the travel range of the device. To estimate the theoretical resolution of the designed system, a numerical model of the MEMS system was established. Detailed information of the numerical modeling approach is given in our earlier works [12]. The model predicted that the comb fingers are capable of moving ±53 μm at 28 V (figure 8). According to (9), this yields a theoretical spectral resolution of around 0.4 nm at 500 nm and 3.6 nm at 1.5 μm wavelengths.

The grating period is 145 μm, which yields a diffraction angle about 7 mrad. If the number of illuminated periods is sufficiently large, isolated monitoring of the zeroth order is easily achievable. In our system, more than ten grating periods are illuminated and diffraction orders are well separated.

5. Experimental results

5.1. Mechanical response

Figure 9(*a*) plots the experimental frequency response within the principal parametric resonance range with sinusoidal excitation, and figure 9(*b*) shows the excitation and oscillation waveforms at the peak of the resonance curve for square-wave excitation. Effects of the parametric nature of the system can be observed from both figures. The principal resonance is located around twice the natural frequency of the z-translation mode even though the actual device oscillates at its eigenmode; this phenomenon is called *subharmonic oscillation* and is a characteristic of parametrically excited systems. Moreover, the frequency response of the spectrometer shows a hysteretic behavior. The amplitude of the oscillations makes sudden jumps at two different frequencies. Oscillations between

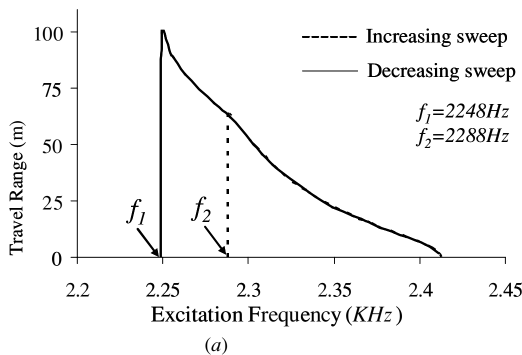

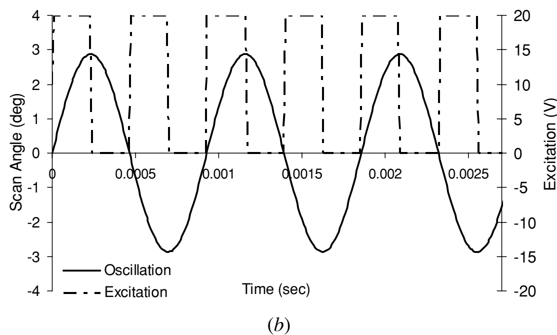

Figure 9. (*a*) Hysteretic frequency response of the spectrometer with 28 V sinusoidal excitation within the primary parametric resonance range. The actual device oscillations are of half the excitation frequency. Maximum amplitude is observed at the first jump frequency f_1, which is equal to about twice the eigenmode frequency. (*b*) Excitation versus device oscillation at the peak of the resonance curve. The excitation signal is chosen as a square wave for better observation of subharmonic oscillations.

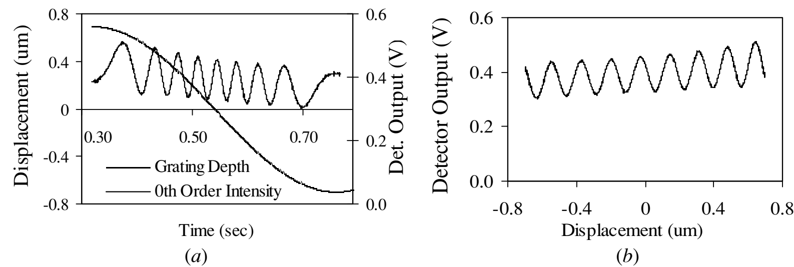

Figure 10. (*a*) Modulation of the zeroth order intensity w.r.t. time with monochromatic illumination (experimental data). (*b*) Modulation of the zeroth order intensity w.r.t. finger position calculated from 10(*a*).

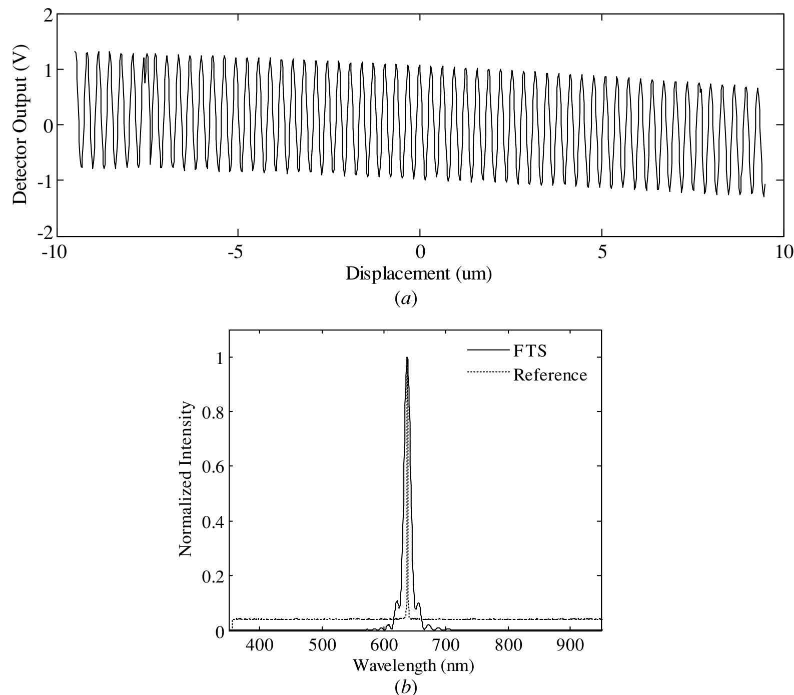

Figure 11. (*a*) Experimental detector signal versus optical path difference for a travel range of 19 μm. (*b*) Comparison of spectral measurements performed with the FTS and a commercial spectrometer.

the two jump frequencies can only be excited if the external frequency is quasi-statically swept down to this region from above. Similar system dynamics are also observed in torsional comb-actuated microscanner devices and were studied in detail in [12]. At the peak of the frequency response curve, the device is capable of producing ± 53 μm vertical deflection with 28 V sinusoidal excitation, which is in very good agreement with the numerical simulations. However, for stable operation, the device should be operated slightly to the right of the resonance peak, since electrical or mechanical impulses might cause oscillations to vanish. Similar devices were tested in open loop for raster-scanning display applications and the oscillations were found to be stable. A closed-loop system with a position sensing mechanism can be used for better frequency and phase stability.

The spectrum data can only be calibrated by the accurate measurement of the deflection amount with sub-wavelength precision, which requires a position sensor. Mechanical characterization of the structure and spectral measurements presented in this paper are performed using a Polytec PDV100 laser Doppler vibrometer. A compact, simple and accurate solution for the position feedback problem is illuminating the backside of the device with a known calibration source and monitoring the 0th and +1st diffraction orders with two photodetectors. Thus, the comb actuators can be utilized for a third function, in addition to actuation and variation of the grating depth. Position sensing systems using this method have reported to resolve deflections in pico meter range [15].

5.2. Spectral measurements

Spectrum measurements are performed with a single photodetector placed at zeroth order. Due to the resonant motion of the device, the speed of the movable fingers is not constant, but sinusoidally varying. Therefore, the recorded detector intensity for a monochromatic source is a chirped (i.e. varying frequency) sinusoid. Figure 10(*a*) shows this chirped modulation of zeroth order intensity for a half-period movement of the fingers. The maximum travel range is chosen to be very small (1.45 μm), so that the modulation frequency is low and the chirping effect is clearly visible. The

frequency of the chirped signal is the lowest at the extremities of the deflection where the velocity is low. The actual cosine modulation of the intensity w.r.t. the finger position $I(d)$ is plotted in figure 10(*b*).

$I(t)$ and $d(t)$ given in figure 10(*a*) are obtained by an A/D conversion which samples the continuous intensity and position signals at uniform time intervals. However, $I(d)$ of figure 10(*b*) consists of non-uniformly spaced samples. In order to obtain a uniformly sampled $I(d)$ data, an interpolation and resampling algorithm is used before the Fourier transform operation to obtain the spectrum. An alternative is to use a non-uniform sampling clock which can be generated using the electronic drive signal or using the optical feedback obtained by an additional monochromatic source and a detector, which provides a simple and elegant solution to the problem [3, 16].

Figure 11(*a*) plots experimental detector output versus optical path difference data. The measured source was a red laser diode and the total travel range of the fingers was 19 μm. Beyond this range, the detector bandwidth was exceeded and the amplitude of the oscillations in figure 11(*a*) was modulated, leading to the broadening of the measured spectral peak. This problem can easily be overcome by using a faster detector. In figure 11(*b*) the spectrum of the light measured with the FTS and a commercial spectrometer are compared. The FTS result is obtained by the Fourier transforming of the data in figure 11(*a*). The sinc shape of the measured peak is due to the rectangular window of the Fourier transformed signal data as given in (7). The peak wavelength is measured to be 639 nm with the FTS, while the reference measurement result is 638 nm. High resolution position feedback of the vibrometer ensures that the peak wavelength is located within a good accuracy. However, the measured FWHM is 12.2 nm, and it is slightly more than twice the theoretical value (5.8 nm). Light collection efficiency is measured to be 15%, which is significantly lower than the theoretical value. The fundamental reason behind the efficiency degradation is the static flatness problem associated with the comb fingers acting as a grating even in the static position. Dynamic deformation is not an issue in this design. Static flatness problems can be corrected by adjusting the Al deposition process parameters.

6. Conclusions

Design, fabrication and characterization of an out-of-plane vertical comb-drive actuator based Fourier transform spectrometer with 3 mm × 3 mm clear optical aperture is discussed. The device is capable of producing ±52 μm vertical deflection at 28 V square-wave excitation without requiring vacuum packaging. This performance level yields a theoretical spectral resolution of about 0.4 nm in the visible band and 3.6 nm at telecom wavelengths. The device is also suitable for spectroscopy in the mid and the long wave IR bands. The device fabrication is simple and uses the standard SOI process with three masks and does not require additional IR optics. The only moving part is the resonating MEMS structure. Since the comb-fingers are used both for actuation and as dynamic diffraction grating, the die is not much larger than the optical aperture. This minimizes the size, complexity, cost and the design effort of a fully functional system. An operational spectrometer using this die requires integration with a simple photodetector and associated readout circuitry. The spectrometer has a number of unique features and important advantages compared to other MEMS spectrometers discussed earlier [3–5].

Acknowledgments

The authors would like to thank Dr Harald Schenk for sharing his experience on micro-spectrometers and Zeljko Skokic for his help on the mask design.

References

[1] Griffiths P R 1986 *Fourier Transform Infrared Spectrometry* (New York: Wiley)
[2] Strong J and Vanasse G A 1960 Lamellar grating far-infrared interferomer *J. Opt. Soc. Am.* **50** 113
[3] Kenda A, Drabe C, Schenk H, Frank A, Lenzhofer M and Scherf W 2006 Application of a micromachined translatory actuator to an optical FTIR spectrometer *Proc. SPIE* **6186** 618609
[4] Schenk H, Groger H, Zimmer F, Scherf W and Kenda A 2005 Optical MEMS for advanced spectrometers *Proc. IEEE/LEOS Conf. on Optical MEMS* pp 117–18
[5] Manzardo O, Michaely R, Schadelin F, Noell W, Overstoltz T, de Rooij N F and Herzig H P 2004 Miniature lamellar grating interferometer based on silicon technology *Opt. Lett.* **29** 1437–9
[6] Manzardo O, Michaely R, Schadelin F and Herzig H P 2003 Micro-sized spectrometer based on a lamellar grating interferometer *Proc. IEEE/LEOS Conf. on Optical MEMS (Hawaii, USA)* pp 175–176
[7] Overstolz T, Niederer G, Noel W, Gale M T, Herzig H P, Obi S, Thiele H and De Rooij N F 2004 MEMS tunable filter for telecom applications *SPIE Proc.* **5455** 240–51
[8] Schenk H, Dürr P, Haase T, Kunze D, Sobe U, Lakner H and Kück H 2000 Large deflection micromechanical scanning mirrors for linear scans and pattern generation *J. Sel. Top. Quantum Electron.* **6** 715–22
[9] Urey H 2004 MEMS scanners for display and imaging applications *Proc. SPIE* **5604** 218–29
[10] Sun Y, Piyabongkarn D, Sezen A, Nelson B J and Rajamani R 2002 A high-aspect-ratio two-axis electrostatic microactuator with extended travel range *Sensors Actuators* A **102** 49–60
[11] Urey H, Kan C and Davis W O 2005 Vibration mode frequency formulae for micromechanical scanners *J. Micromech. Microeng.* **15** 1713–21
[12] Ataman C and Urey H 2006 Modeling and characterization of comb actuated resonant microscanners *J. Micromech. Microeng.* **16** 9–16
[13] Turner K L, Miller S A, Hartwell P G, MacDonald N C and Strogatz S H 1998 Five parametric resonances in a microelectromechanical system *Nature* **396** 149–52
[14] Baskaran R and Turner K 2003 Mechanical domain coupled mode parametric resonance and amplification in a torsional mode micro electro mechanical oscillator *J. Micromech. Microeng.* **13** 701–7
[15] Lee W, Hall N A, Zhou Z and Degertekin F L 2004 Fabrication and characterization of a micromachined acoustic sensor with integrated optical readout *IEEE J. Sel. Top. Quantum Electron.* **10** 643–51
[16] Ataman C, Isikman S O, Urey H and Wolter A 2006 MEMS based visible-NIR Fourier transform microspectrometer *Proc. SPIE* **6186** 61860C